ACES Asian Chemical Editorial Society

DOI: 10.1002/cnma.201600173

CHEMNANOMAT
Full Paper

Electrocatalysts

In Situ Growth of Co_3O_4 Nanoparticles on Interconnected Nitrogen-Doped Graphene Nanoribbons as Efficient Oxygen Reduction Reaction Catalyst

Hengyi Lu,[a] Jiajie Yan,[a] Youfang Zhang,[a] Yunpeng Huang,[a] Wei Gao,[a] Wei Fan,*[b] and Tianxi Liu*[a, b]

Abstract: A simple, low cost and nontoxic preparation method to obtain high performance oxygen reduction reaction (ORR) catalysts is of great significance in fuel cell fields. Herein, graphene nanoribbons (GNRs) with numerous graphitic edges are chosen as supporting material to hybridize with nitrogen atoms and cobalt oxide (Co_3O_4) through a simple one-step hydrothermal reaction. With a high edge-to-plane ratio, the GNR sheets could increase the accessibility of N-atom doping into the graphene edges to form active ORR sites, and be also interconnected with each other to form a conductive network, thus facilitating the fast electron transfer. The intimate contacts between Co_3O_4 nanoparticles and nitrogen-doped GNRs (N-GNRs) along with the porous structure impart the N-GNR/Co_3O_4 hybrid with excellent ORR performance, which leads to a comparable onset-potential to commercial Pt/C catalyst but larger current density, better long-term stability and superior tolerance to crossover effects.

Introduction

Fuel cells can convert the chemical energy in fuels like hydrogen or methanol into electricity without any toxic byproducts, but their efficiency is greatly limited by the sluggish kinetics of the cathode oxygen reduction reaction (ORR).[1] Therefore, developing high-efficiency, high-durability and low-cost ORR catalysts is of great importance in the advancement of fuel cells. To date, commercial ORR catalysts rely greatly on Pt-based materials because of their extraordinary ORR activity. However, their disadvantages such as poor durability, high cost and susceptibility to crossover effects severely hinder their wide application.[2] In recent years, great efforts have been devoted to search for nonprecious metal alternatives, and among them, carbon-based nanomaterials have been recognized as promising candidates to replace the Pt/C catalyst.[3–6]

Among various carbon materials, graphene and carbon nanotubes (CNTs) are considered to be suitable substrates for heteroatom doping or immobilization of electrochemically active nanomaterials due to their intrinsic excellent conductivity and chemical stability.[3,5,7–9] In addition, the edges of graphene show a much faster electron transfer rate and much higher electrocatalytic activity than the basal plane according to some previous experimental results and density function theory calculations.[10–13] Since O_2 molecules are more likely to be adsorbed on the exposed edges of graphene rather than the basal plane itself, graphene edges result in higher ORR activity.[14] Many studies show that the doping of nonmetal heteroatoms (like N atom) into graphene or CNTs can greatly enhance their ORR catalytic activity because heteroatom doping can change the electronic and surface chemical properties of these carbon materials.[3,5,15,16] Additionally, the incorporation of N atoms into carbon can also increase the electronic density of states near the Fermi level, thus facilitating the electronic transfer from the C to O as well as the O=O breaking in O_2.[3,12] Furthermore, the N atoms located at graphitic edges also show higher ORR activity, for the ORR-active pyridinic N and pyrrolic N are both located at the edges of graphene plane.[17,18]

As a new sibling of graphene, graphene nanoribbons (GNRs) have quasi-one-dimensional structure and much higher edge-to-plane ratio than graphene sheets.[19,20] The basal plane of GNRs consisted of conjugated sp^2 carbon atoms could retain the unique properties of graphene, while the edges containing a defective graphitic line of carbon atoms with dangling bonds and various capping moieties (e.g., hydroxyl, carbonyl and carboxyl groups) can also provide many electrochemically active

[a] H. Lu, J. Yan, Y. Zhang, Y. Huang, W. Gao, Prof. T. Liu
State Key Laboratory of Molecular Engineering of Polymers
Department of Macromolecular Science
Fudan University
220 Handan Road, Shanghai 200433 (P. R. China)
E-mail: txliu@fudan.edu.cn
txliu@dhu.edu.cn

[b] Dr. W. Fan, Prof. T. Liu
State Key Laboratory for Modification of Chemical Fibers and Polymer Materials
College of Materials Science and Engineering
Donghua University
2999 North Renmin Road, Shanghai 201620 (P. R. China)
E-mail: weifan@dhu.edu.cn

Supporting information for this article can be found under http://dx.doi.org/10.1002/cnma.201600173.

sites.[10] Therefore, GNRs with abundant edges and high-conductivity features could be promising supporting materials for ORR catalysts. However, up to now, reports on GNRs-based ORR catalysts are far fewer than that of graphene-based materials. In addition, most of the GNRs-based ORR catalysts in the literature are confined to chemical doping, like N-doping[21] or B, N co-doping,[22,23] which shows limited improvement of ORR activity. As far as we know, there are only few reports on the hybridization of N-doped GNRs with metal oxides for ORR catalytic applications.

In this work, GNRs obtained from longitudinal unzipping CNTs were used as supporting materials for both N-atom doping and anchoring of Co_3O_4 nanoparticles to prepare N-GNR/Co_3O_4 hybrids through a simple one-step hydrothermal reaction. During the hydrothermal process, the reduction of graphene oxide nanoribbons (GONRs), the doping of nitrogen and in situ growth of Co_3O_4 nanoparticles on GONRs were realized simultaneously. When used as an ORR catalyst, N-GNR/Co_3O_4 hybrids manifest comparable onset potential to commercial Pt/C catalyst, along with slightly larger current density, improved stability and superior resistance to crossover effects.

Results and Discussion

Synthesis and characterization of GONRs and N-GNR/Co_3O_4 hybrids

GONRs were first prepared by longitudinally unzipping pristine MWCNTs according to previous work.[19] The TEM images in Figure 1 show the diameter of pristine MWCNTs is 20–50 nm while the width of GONRs is 80–150 nm after chemically unzipping. Some GONR fragments were also observed due to sonication aiming to disperse GONRs in water, as shown in Figure 1e. Once the GONR dispersion (1 mg mL^{-1}) was obtained, $Co(CH_3COO)_2{\cdot}4H_2O$ aqueous solution was added dropwise under sonication followed by stirring for 30 min (Scheme 1). In this manner, Co^{2+} would be absorbed on the surface of GONRs due to the electrostatic interactions between the oxygen-containing groups and metal cations. Then $NH_3{\cdot}H_2O$ was added into the suspension, and $[Co(NH_3)_6]^{3+}$ was formed and decomposed at a certain temperature to generate Co_3O_4 nanoparticles.[23] The advantage of this synthetic method is that excessive $NH_3{\cdot}H_2O$ can act as a nitrogen source for N-doping of GONRs. After stirring for another 10 min under ambient condition, the mixture was transferred into Teflon autoclave followed by a hydrothermal process. The final black products (i.e., N-GNR/Co_3O_4 hybrids) were collected by centrifugation and washed with water and alcohol, and then used as ORR catalyst.

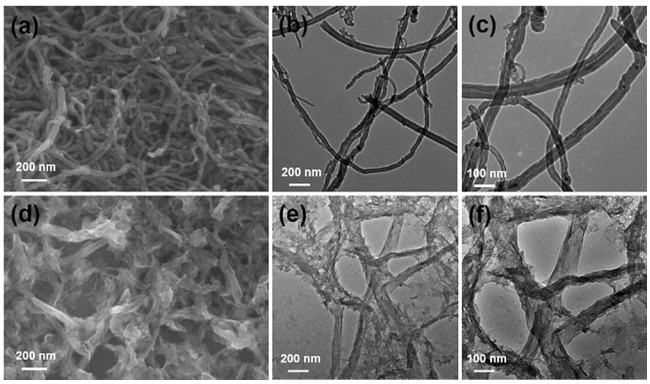

Figure 1. FESEM and TEM images of (a, b, c) CNTs and (d, e, f) GONRs.

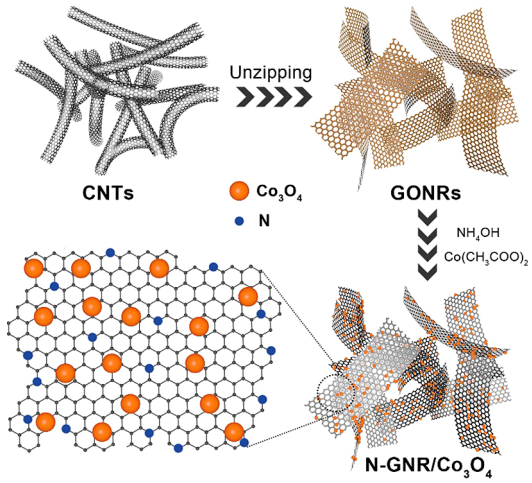

Scheme 1. Preparation procedure for the N-GNR/Co_3O_4 hybrids.

The successful preparation of N-GNRs/Co_3O_4 hybrid can be seen by TEM. As shown in Figure 2a and 2b, Co_3O_4 nanoparti-

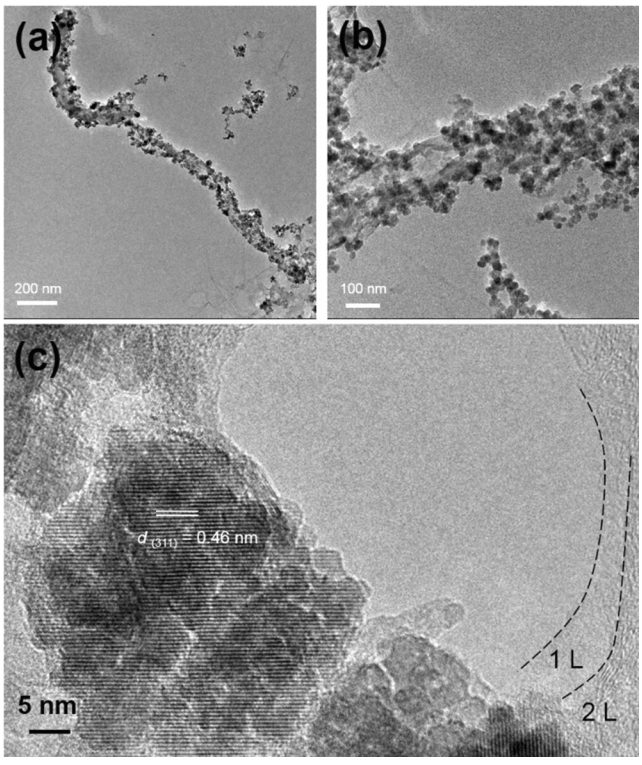

Figure 2. TEM images of N-GNR/Co_3O_4 hybrid at low (a) and high (b) magnifications and corresponding HRTEM images (c).

cles are uniformly anchored on N-GNRs with small size of 5–10 nm, and this small-sized Co_3O_4 can offer more ORR active sites for electrochemical applications. The HRTEM image (Figure 2c) clearly shows the lattice fringe of Co_3O_4 nanoparticles, which confirm that crystalline structures are formed. Figure 2c also shows few-layered GNRs with no obvious stacking or agglomerations in the N-GNR/Co_3O_4 hybrid, which is due to the fact that immobilization of Co_3O_4 nanoparticles on GNR planes can effectively prevent their aggregation during the reduction process, thus resulting in the full utilization of the large surface area of GNRs. The scanning TEM image and corresponding elemental mapping analysis of N-GNR/Co_3O_4 suggest the presence and uniform distribution of C, Co, O, N in the hybrid (Figure S1 in the Supporting Information). The FESEM images of N-GNR/Co_3O_4 hybrids with different Co_3O_4 loading contents are shown in Figure S2. All the samples display good distribution of Co_3O_4 nanoparticles on the surface of GNR sheets. However, overloading of Co_3O_4 nanoparticles will lead to their aggregation (Figure S2c and S2d) and may block the active centers, thus leading to lower ORR performance.

Figure 3a reveals the increase of the intensity ratio of D band to G band in GONRs ($I_D/I_G = 0.97$) compared with CNTs

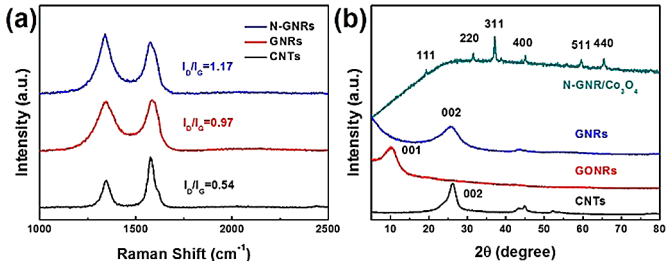

Figure 3. (a) Raman spectra of CNTs, GNRs and N-GNRs. (b) XRD patterns of CNTs, GONRs, GNRs and N-GNR/Co_3O_4 hybrid.

($I_D/I_G = 0.54$), indicating the existence of substantial defect edges in GONRs. Figure 3b displays the XRD patterns of CNTs, GONRs, GNRs and N-GNR/Co_3O_4 hybrid. The sharp (002) graphitic peak at $2\theta = 26.1^\circ$ of CNTs corresponds to the *d*-spacing of 3.4 Å, which is the characteristic interlayer spacing of CNTs. For GONRs, the sharp (002) peak was substituted by a broad (001) peak centered at $2\theta = 10.2^\circ$ corresponding to a *d*-spacing of 8.7 Å. The increased *d*-spacing is caused by the insertion of oxygen-containing groups during the unzipping process, which is supported by XPS and TGA analysis of pristine CNTs and GONRs. As shown in Figure S3, both the XPS and TGA data show an obvious increase in the number of oxygen-containing groups after the unzipping process. The disappearance of (001) peak and the reappearance of (002) peak in the XRD pattern of GNRs indicate a reduction process occurred and the GONRs have been reduced to GNRs during the hydrothermal reaction. This phenomenon is similar to the XRD pattern changes when graphene oxide (GO) is reduced to graphene (rGO). The diffraction pattern of N-GNR/Co_3O_4 exhibits a set of characteristic peaks at $2\theta = 19.1^\circ$, 31.5°, 37.1°, 44.9°, 59.5° and 65.3° corresponding to the (111), (220), (311), (400), (511), (440) crystal facets of cubic spinel-structured Co_3O_4 (JCPDS no. 42-1467). The characteristic peak originating from GNRs is invisible in this pattern, which is probably due to the strong peaks of the metal oxide that may hind the broad peak of carbon materials.

In order to analyze the surface elemental composition and the chemical state of each element in N-GNR/Co_3O_4, XPS characterization was performed (Figure 4). The survey spectrum

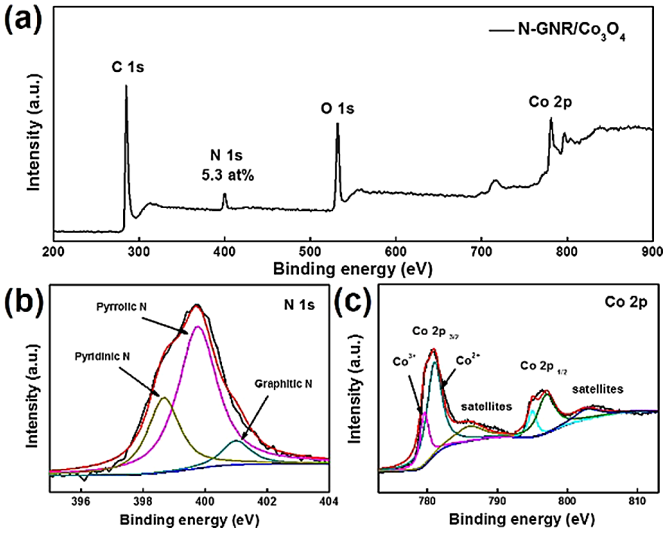

Figure 4. (a) Survey XPS spectra of N-GNR/Co_3O_4 hybrid. High resolution (b) N 1s spectrum and (c) Co $2p_{3/2}$ spectrum.

shows the contents of C, N, O and Co elements in the hybrid are 71.71 at%, 5.26 at%, 19.04 at% and 3.99 at%, respectively. The presence of the N 1s peak confirms the successful doping of nitrogen atoms into the carbon substrate. It is worthwhile to note that the ORR performance is strongly dependent on the bonding configuration of N atoms.[12,18,24] The high resolution N 1s peak (Figure 4b) reveals that the nitrogen atoms are incorporated into the carbon structure in three main configurations: pyridinic N (398.6 eV, 28 at%), pyrrolic N (399.7 eV, 64 at%) and graphitic N (401.0 eV, 8 at%). Both pyridinic N and pyrrolic N are located at the graphitic edge. Each pyridinic N is bonded to two carbon atoms and donates one p-electron to the aromatic π system while pyrrolic N atoms are integrated into five-membered heterocyclic rings and contribute two p-electrons to the π system. Quaternary N atoms are those doping into the hexagonal carbon atom rings.[15,18,25] Although the real nature of various N sites is still uncertain, there is a widely accepted view that the N atoms located at the graphitic edge are much more active than the in-plane N doped sites for ORR.[17,26] The abundant edges in GNRs greatly increase the amount of N atoms doping into the edge graphitic carbon, thus potentially leading to a better performance.

The Co 2p spectrum of N-GNR/Co_3O_4 hybrid exhibits two main peaks at 796.4 eV and 780.5 eV, corresponding to Co $2p_{1/2}$ and Co $2p_{3/2}$, respectively (Figure 4c). Moreover, there are two weak satellite peaks besides the main peaks, all confirming the formation of Co_3O_4 phase.[27] The deconvolution of Co $2p_{3/2}$

shows two main peaks at 779.8 eV and 781.2 eV, respectively corresponding to Co^{3+} and Co^{2+} species, with a weak satellite peak at around 786.0 eV.[28,29] The higher Co^{2+} content indicates that Co^{3+} is partly reduced in the N-GNR/Co_3O_4, which may be due to a strong covalent interaction between Co_3O_4 and N-GNR.[29,30] Nitrogen sites have been proved to be anchoring sites for Co_3O_4 nanoparticles through the formation of C–O–Co and C–N–Co bonds at the oxide/carbon interface by X-ray absorption near edge structure (XANES) and DFT calculations in previous works, and the C–O–Co and C–N–Co bonds likely play an important role in improving the electrocatalytic activity.[7,29,31–33]

Electrochemical tests of ORR performance

The ORR performance of different samples is investigated by cyclic voltammetry (CV) and linear sweep voltammetry (LSV) in O_2 saturated 0.1 M KOH electrolyte solution (Figure 5). All the samples show well-defined cathodic redox peaks that correspond to the O_2 reduction process in electrolyte solution. As is well-known, more positive peak potential and larger peak current density mean better ORR performance. As shown in Figure 5a, the reduction peak of N-GNRs is located at 0.78 V, which is more positive than that of GNRs (0.71 V). This result indicates that the doping of nitrogen could significantly improve the electrocatalytic activity of GNRs, which is consistent with previous reports.[15,18,23,34] Further introduction of Co_3O_4 nanoparticles leads to a much higher peak potential (0.86 V) and larger peak current density. The significant improvement stems from the efficient coordination between Co_3O_4 and N-GNR, since the C–O–Co and C–N–Co bonds have been proved to be ORR active centers.[7,29,35,36] Furthermore, N-GNR/Co_3O_4 hybrid shows superior ORR activity to N-CNT/Co_3O_4 and N-rGO/Co_3O_4 hybrids in terms of more positive onset potential and larger current density, indicating the important role of GNRs in the synergistic reinforcement of electrochemical activity (Figure 5b). Specifically, abundant active edges of GNRs provide numerous anchoring sites for growth of metal oxide and nitrogen doping, thus resulting in a larger surface area and greatly increased active sites in the hybrids. As shown in Figure S4, the BET surface area of N-GNR/Co_3O_4, N-rGO/Co_3O_4 and N-CNT/Co_3O_4 are 105.5, 81.8 and 69.4 $m^2 g^{-1}$, respectively. Additionally, the high edge-to-plane ratio of GNR sheets could increase the accessibility of N atoms doping into the graphene edges to form more pyridinic N (28 at%) and pyrrolic N (64 at%) in N-GNR/Co_3O_4, which have been previously reported to be more active ORR sites than graphitic N. In addition, GNRs interconnected with each other to form a conductive network, thus facilitating the fast electron transfer within the N-GNRs/Co_3O_4.

To optimize the performance of N-GNR/Co_3O_4 hybrids, the dosages of $Co(CH_3COO)_2{\cdot}4H_2O$ are set as 0.1, 0.2, 0.3 and 0.4 mmol, and the corresponding hybrids are denoted as N-GNR/0.1 Co_3O_4, N-GNR/0.2 Co_3O_4, N-GNR/0.3 Co_3O_4 and N-GNR/0.4 Co_3O_4, respectively. Figure 5c reveals that different samples exhibit almost the same peak potential while the peak current density shows a volcanic change trend, suggesting the number of active centers varies with different loading contents of Co_3O_4 in N-GNR/Co_3O_4 hybrids, which further affects electrocatalytic activity. LSV curves in Figure 5d corresponds well with the CV results, with N-GNR/0.2 Co_3O_4 showing the largest current density. The reason can be inferred from Figure S2; the

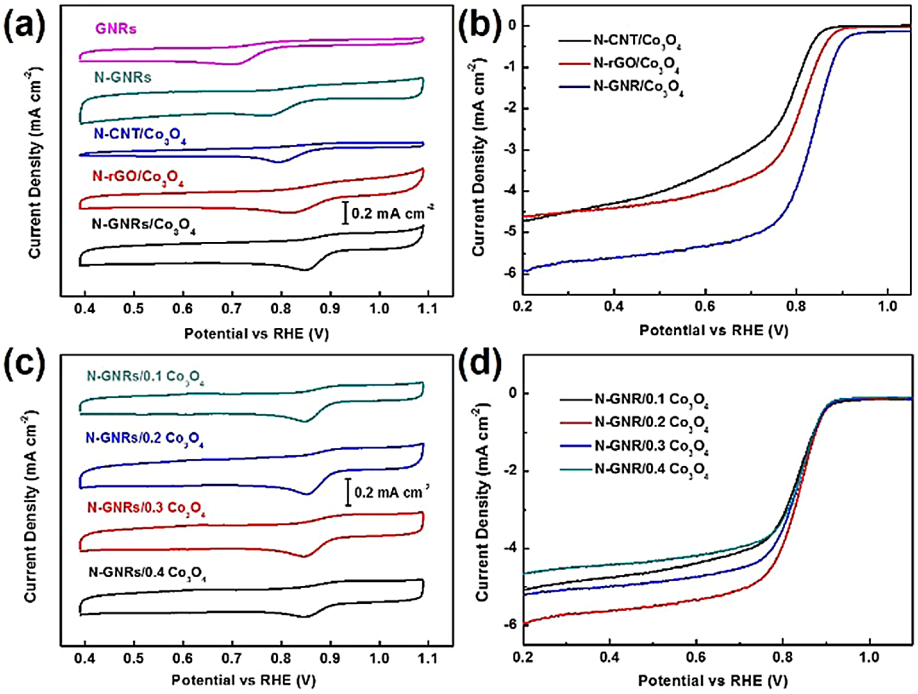

Figure 5. (a,c) CV curves and (b,d) LSV curves of different samples in O_2-saturated 0.1 M KOH solution at 1600 rpm.

high content of Co_3O_4 will cause aggregation and hinder some ORR active centers. Since N-GNR/0.2 Co_3O_4 shows the largest current density among the hybrid samples, the following ORR performance tests are conducted on this sample. The content of Co_3O_4 in this hybrid was calculated to be 55.8 wt% from TGA results (Figure S5).

The LSV measurements were performed in O_2-saturated 0.1 M KOH at a scan rate of 5 mV s^{-1} to further evaluate the electrocatalytic activity and kinetics of the catalysts. Figure 6a shows a series of LSV curves of N-GNR/0.2 Co_3O_4 hybrid obtained on a rotating disk electrode (RDE) at rotating rates ranging from 400 rpm to 2025 rpm. The oxygen reduction current density increases with the increase of rotation rate due to enhanced mass transportation and shortened diffusion distance.[37,38] The Koutecky–Levich (K–L) equation is utilized to analyze the kinetic parameters (Figure 6b). The good linearity of the K-L plots and nearly parallelism of the fitting lines indicate that the ORR process catalyzed by N-GNR/0.2 Co_3O_4 hybrid obeys the first-order reaction kinetics with regard to the concentration of dissolved oxygen and similar electron transfer numbers (n) at various potentials.[7,39] The electron transfer number of N-GNR/0.2 Co_3O_4 hybrid was calculated to be 3.96 from the K-L plots from 0.3 V to 0.7 V, indicating a predominant complete 4 e^- reduction process. Rotating ring-disk electrode (RRDE) measurements were further performed to monitor the formation of peroxide species (HO_2^-) during the ORR process to verify the ORR catalytic pathways of N-GNR/Co_3O_4 (Figure 6c). The measured HO_2^- yields are below ≈8% over the potential range of 0.2–0.80 V, giving an electron transfer number of ≈3.9 (Figure 6d). This is consistent with the result obtained from the Koutecky–Levich plots based on RDE measurements, suggesting the ORR catalyzed by our hybrids is mainly by 4 e^- reduction.

Figure 6e represents the LSV curves of GNRs, N-GNRs, N-GNR/0.2 Co_3O_4 and commercial Pt/C catalysts in O_2-saturated 0.1 M KOH at a rotating rate of 1600 rpm. The onset potential

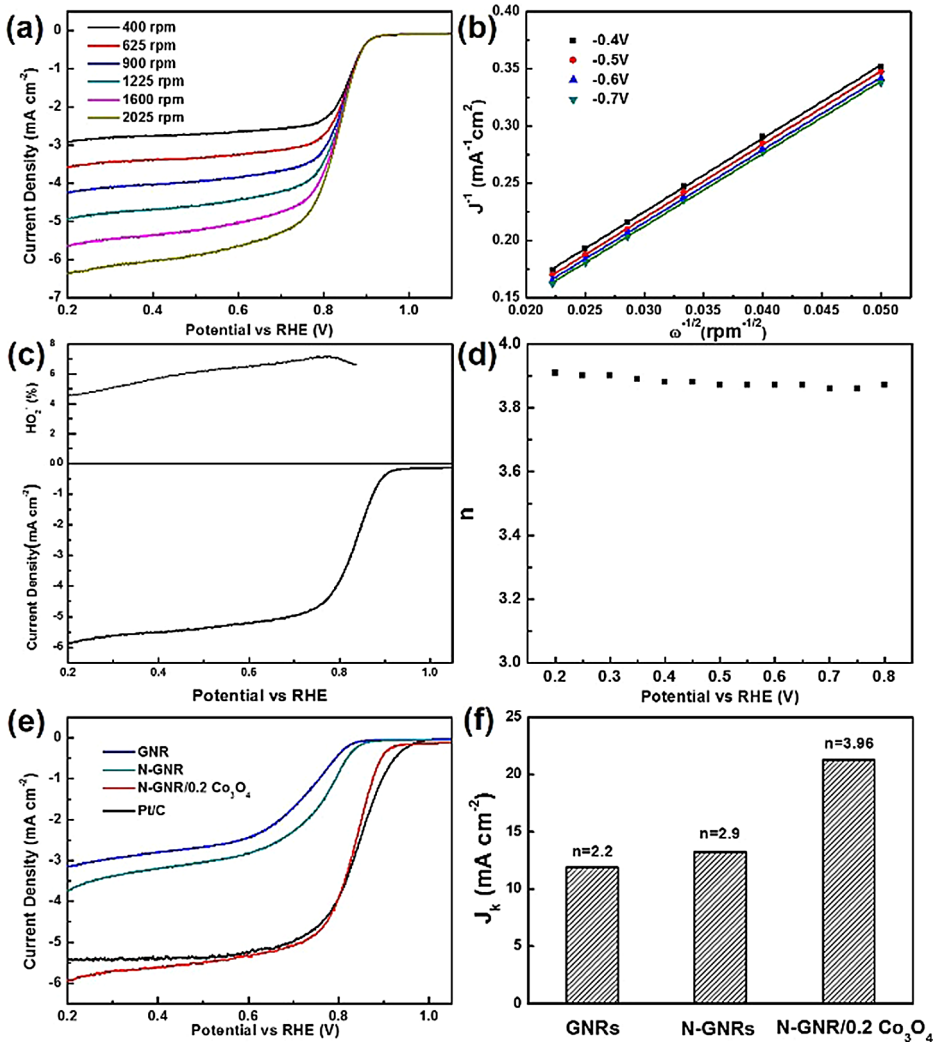

Figure 6. (a) RDE voltammograms of N-GNR/0.2 Co_3O_4 hybrid in O_2 saturated 0.1 M KOH at rotation rates from 400 rpm to 2025 rpm. (b) K-L plots of the N-GNR/0.2 Co_3O_4 hybrid. (c) RRDE measurements showing peroxide yield at a rotation rate of 1600 rpm. (d) Number of electrons per oxygen molecule transferred during ORR. (e) RDE voltammograms of different samples in O_2-saturated 0.1 M KOH at rotation rate of 1600 rpm. (f) Electron transfer number and kinetic current density of different hybrids.

of N-GNRs (0.89 V) is much higher than that of GNRs (0.83 V), while the kinetic-limiting current density only shows slight improvement, which is probably due to the configuration of doped nitrogen in the GNRs. As reported previously, pyridinic N and pyrrolic N, both of which are located at graphitic edges, mainly affect the onset-potential rather than the current density.[18,40] The abundant edges in GNRs may increase the amounts of these N atoms, so N-GNRs show an obvious improvement in onset potential rather than current density. As for N-GNR/0.2 Co_3O_4, this hybrid has a comparable onset potential and slightly larger current density than Pt/C catalyst. The electron transfer number and kinetic-limiting current density of different samples are calculated from Figure S6, Figure S7 and Figure 6b, among which N-GNR/0.2 Co_3O_4 shows the largest current density of 21.3 mA cm^{-2} (Figure 6f).

Long-term stability is another important property for ORR catalysts, which is what the commercial Pt/C catalyst lacks. The durability of the N-GNR/0.2 Co_3O_4 is tested by chronoamperometric measurement under a constant potential of 0.6 V in O_2-saturated 0.1 M KOH at an electrode rotation rate of 1600 rpm. As shown in Figure 7a, the N-GNR/0.2 Co_3O_4 exhibits an excellent durability with an almost 95% retention of current density after continuously working for 40000 s. For comparison, Pt/C tested under the same conditions shows a 35% decrease. The excellent long-term stability of N-GNR/Co_3O_4 hybrid stems from the carbon supporting materials that could help anchor Co_3O_4 nanoparticles, thus suppressing the dissolution of active sites. The TEM images of N-GNR/Co_3O_4 hybrid after long-term stability tests (Figure S8) show the structure of N-GNR/0.2 Co_3O_4 remains almost the same as before the cycling test, except the size of Co_3O_4 nanoparticles increased slightly. No obvious agglomeration of GNR or Co_3O_4 nanoparticles could be observed from the TEM images.

Some fuel molecules may penetrate through electrolyte membrane and react with cathode ORR catalysts thus deteriorating the efficiency of fuel cells in practical applications, which is the so-called fuel crossover effect. The resistance to methanol of N-GNR/0.2 Co_3O_4 is evaluated by recording the current-time chronoamperometry when methanol is introduced during the ORR process (Figure 7b). The current of Pt/C changes instantaneously while the current of N-GNR/0.2 Co_3O_4 remains almost the same upon the addition of methanol. Furthermore, the CVs of N-GNR/0.2 Co_3O_4 overlap well before and after the introduction of methanol, revealing the excellent tolerance to methanol crossover effects for N-GNR/Co_3O_4 hybrid (Figure 7c). In contrast, Pt/C catalyst completely lost its ORR activity (Figure 7d). All these results confirm that the N-GNR/Co_3O_4 hybrid could be a promising alternative for commercial Pt/C catalyst.

Conclusions

In summary, a simple one-step hydrothermal method is developed to fabricate nitrogen-doped graphene nanoribbon/Co_3O_4 nanoparticle hybrids, during which the NH_4OH not only reacts with Co^{2+} to form the intermediate of Co_3O_4, but also serves as a nitrogen source for the N-doping. GONRs provide abundant edges for N-atom doping into the edges of graphitic carbon to form efficient N sites for ORR, as well as plentiful an-

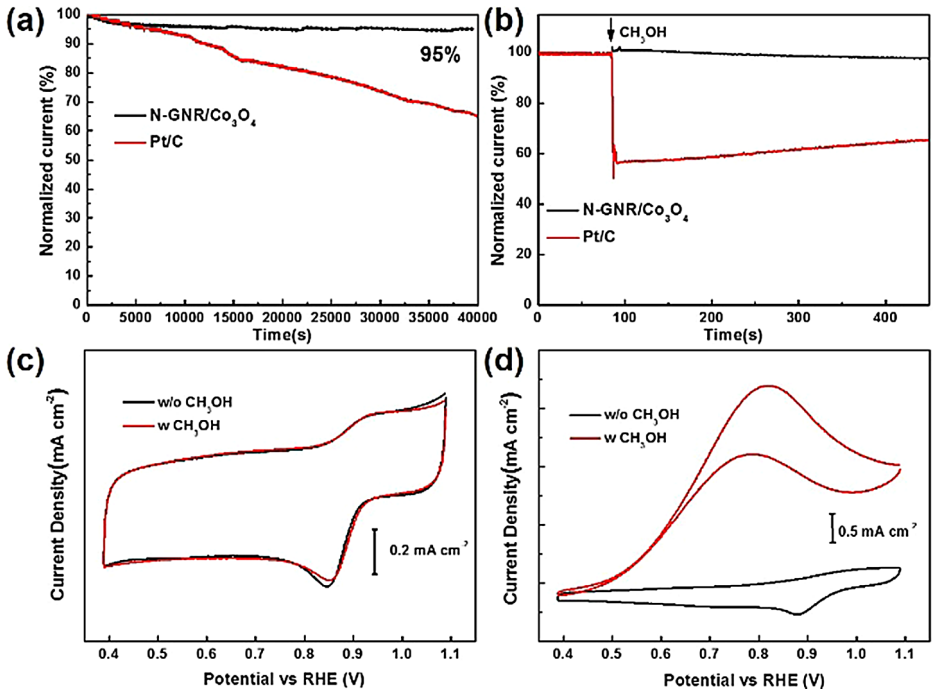

Figure 7. Chronoamperometric responses of N-GNR/Co_3O_4 hybrid and Pt/C catalyst at −0.4 V (vs. Ag/AgCl) (a) in O_2 saturated 0.1 M KOH electrolyte, and (b) with the quick injection of methanol with a rotation rate of 1600 rpm. CV curves of (c) N-GNR/Co_3O_4 and (d) Pt/C hybrid before and after the addition of methanol.

choring sites for metal oxides. In the final N-GNR/Co_3O_4 hybrid products, the interconnected GNR sheets could form electron-transfer pathways and increase the conductivity, and the intimate interplay between N-GNRs and Co_3O_4 nanoparticles imparts the hybrids impressive ORR catalytic performance. In addition, the N-GNR/Co_3O_4 hybrids also show excellent long-term stability and resistance to methanol crossover effects. This work provides a new strategy for developing GNRs-based ORR catalysts.

Experimental Section

Materials

Multi-walled carbon nanotubes (MWCNTs, 95%, 20–50 nm in diameter; ≈20 μm in length, produced by the CVD method) were obtained from Chengdu Organic Chemicals Co. Ltd. 98% H_2SO_4, 30% H_2O_2, 37% HCl, 25% NH_4OH, 85% H_3PO_4, *N,N*-dimethylformamide (DMF), $KMnO_4$, cobalt acetate ($Co(CH_3COO)_2{\cdot}4H_2O$) were supplied by Sinopharm Chemical Reagent Co. Ltd and used without any further treatment. Commercial Pt/C catalyst (Platinum, 20 wt% on carbon black) was purchased from Alfa Aesar.

Preparation of graphene oxide nanoribbons (GONRs)

GONRs were prepared according to literature procedures.[19,21] Briefly, 150 mg of pristine MWCNTs were mixed with 36 mL of 98% H_2SO_4 in a flask and stirred for 60 min to form a uniform suspension. Then, 4 mL of 85% H_3PO_4 was poured into the mixture and stirred for another 30 min. After that, 750 mg of $KMnO_4$ was gradually added into the dispersion under continuous stirring for 60 min. The mixture was then heated at 70 °C for 120 min followed by naturally cooling to room temperature. The reaction mixture was poured into 300 mL ice-water containing 10 mL 30% H_2O_2 and allowed to coagulate for 24 h. The top portion was decanted from the solid. The remaining portion was collected and washed with 5% HCl for 3 times and then dialyzed for a week until the pH was close to 7. The dispersion was vacuum-dried to obtain the GONR solid products. GONR aqueous dispersion (1 mg mL^{-1}) was prepared by sonicating 100 mg GONR solids in 100 mL DI water for 5 min and then gently stirring for 30 min.

Preparation of N-GNR/Co_3O_4 hybrids

N-GNR/Co_3O_4 hybrids were synthesized by a simple one-step hydrothermal reaction. Typically, certain amount of $Co(CH_3COO)_2{\cdot}4H_2O$ was dissolved in 2 mL DI water and then added into 20 mL 1 mg mL^{-1} GONR suspension dropwise. After stirring for 30 min, 4 mL 25% NH_4OH was slowly added into the mixture under vigorous stirring and allowed to stir for another 10 min before a hydrothermal process at 180 °C for 3 h. The black precipitate was collected by centrifugation and subsequently washed with DI water and ethanol for three times and dried at 60 °C for 12 h. The obtained products were denoted as N-GNR/0.1 Co_3O_4, N-GNR/0.2 Co_3O_4, N-GNR/0.3 Co_3O_4 and N-GNR/0.4 Co_3O_4 hybrids when the added amount of $Co(CH_3COO)_2{\cdot}4H_2O$ was 0.1, 0.2, 0.3 and 0.4 mmol, respectively. For comparison, N-GNRs and GNRs were also prepared under the same conditions in the absence of $Co(CH_3COO)_2{\cdot}4H_2O$ or both $Co(CH_3COO)_2{\cdot}4H_2O$ and NH_4OH. And N-CNT/Co_3O_4 and N-rGO/Co_3O_4 hybrids were also prepared according to N-GNR/0.2 Co_3O_4 by substituting GONRs with CNTs or GO (graphene oxide).

Characterization

X-ray diffraction (XRD) measurements were carried out using a PANalytical X'pert PRO XRD with $Cu_{K\alpha}$ radiation (operating voltage, 40 kV; cathode current, 40 mA; $\lambda = 0.1542$ nm; scan rate, 5° min^{-1}). Raman spectra were obtained on a LabRam-1B French Dilor Com ($\lambda = 532$ nm). Transmission electron microscopy (TEM) observation was conducted on a Tecnai G2 F20 S-TWIN TEM instrument under an accelerating voltage of 200 kV. Field emission scanning electron microscopy (FESEM) was performed by a Zeiss Ultra 55 FESEM instrument at an accelerating voltage of 5 kV. X-ray photoelectron spectroscopy (XPS) spectra were collected by a VG ESCALAB 220I-XL device. Thermo-gravimetric analysis (Mettler Toledo TGA1) was carried out with a heating rate of 10 °C min^{-1} from 100 °C to 600 °C in N_2 for CNTs, GONRs and in air for N-GNR/0.2 Co_3O_4 hybrid. The specific surface area of N-CNT/Co_3O_4, N-rGO/Co_3O_4 and N-GNR/Co_3O_4 were characterized with a belsorp-max surface area detecting instrument (Tristar3000) by N_2 physisorption at 77 K.

Electrochemical measurements

All electrochemical measurements were carried out in a conventional three-electrode cell on a CHI 660D electrochemical workstation (Shanghai Chenhua Equipments, China) equipped with a rotating electrode setup (616 A, Princeton Applied Research). To prepare a homogenous catalyst ink, 4 mg of catalyst was first dispersed in 1 mL of mixed solvent of DI water-DMF (v/v = 1/1) with 10 μL Nafion (5 wt%) under sonication. To prepare the working electrode, 5 μL and 10 μL of above suspension was deposited onto polished glassy carbon electrode (GCE, $d = 3$ mm, Shanghai Chenhua Equipments, China) and glassy carbon rotating-disk electrode (RDE, $d = 5$ mm, 616 A, Princeton Applied Research) respectively, followed by drying at room temperature. The electrochemical tests were conducted in O_2 (or N_2)-saturated 0.1 M KOH aqueous solution at room temperature by using Ag/AgCl (3 M) as reference electrode, Pt wire as counter electrode. All the potential was referred to a reversible hydrogen electrode (RHE), $E_{RHE} = E_{Ag/AgCl} + 0.222\ V + 0.059\,pH$. The scan rate was 5 mV s^{-1} for cyclic voltammetry (CV) measurements. All data were recorded after the shapes of CV curves were stable in N_2-saturated 0.1 M KOH. Linear sweep voltammetry (LSV) measurements were carried out at different rotating speed from 400 rpm to 2025 rpm in O_2 saturated 0.1 M KOH solution at a scan rate of 5 mV s^{-1}. The kinetic parameters like electron transfer number (n) and kinetic-limiting current density were calculated according to Koutecky–Levich (K-L) equation:

$$\frac{1}{J} = \frac{1}{J_k} + \frac{1}{J_l} = \frac{1}{J_k} + \frac{1}{B\omega^{0.5}} \quad (1)$$

$$B = 0.2nF(D_0)^{2/3}\nu^{-1/6}C_0 \quad (2)$$

where J is the measured current density, J_k is the kinetic-limiting current density, J_l is the diffusion-limiting current density, ω is the electrode rotation rate (rpm), n is the electron transfer number in ORR, F is the Faraday constant (96485 C mol^{-1}), D_0 is the diffusion coefficient of O_2 in 0.1 M KOH solution (1.9×10^{-5} cm^2 s^{-1}), C_0 is the bulk concentration of O_2 (1.2×10^{-6} mol cm^{-3}), and ν is the velocity of the electrolyte (0.01 cm^2 s^{-1}). The constant 0.2 is used when the rotation rate is expressed in rpm.

For the rotating ring-disk electrode (RRDE) measurements, catalyst inks and electrode were prepared by the same method as RDE's on a ring-disk electrode (RRDE-3 A, BAS Inc.). The disk electrode was scanned cathodically at 5 mV s^{-1} and the ring potential was

constant at 1.25 V versus RHE. The yields of HO_2^- and the electron transfer number (n) were determined by the followed equations:

$$\%HO_2^- = 200 \times \frac{I_r/N}{I_d + I_r/N} \quad (3)$$

$$n = 4 \times \frac{I_d}{I_d + I_r/N} \quad (4)$$

where I_d is the disk current, I_r is the ring current and N is current collection efficiency (0.4) of the Pt ring.[7]

Acknowledgements

The authors are grateful for the financial support from the National Natural Science Foundation of China (51125011, 51433001).

Keywords: doping · fuel cells · graphene nanoribbons · nanoparticles · oxygen reduction reaction

[1] M. Winter, R. J. Brodd, *Chem. Rev.* **2004**, *104*, 4245 – 4270.
[2] X. Ge, A. Sumboja, D. Wuu, T. An, B. Li, F. W. T. Goh, T. S. A. Hor, Y. Zong, Z. Liu, *ACS Catal.* **2015**, *5*, 4643 – 4667.
[3] K. P. Gong, F. Du, Z. H. Xia, M. Durstock, L. M. Dai, *Science* **2009**, *323*, 760 – 764.
[4] M. Zhang, L. M. Dai, *Nano Energy* **2012**, *1*, 514 – 517.
[5] J. Shui, M. Wang, F. Du, L. Dai, *Sci. Adv.* **2015**, *1*, e1400129.
[6] X. J. Zhou, J. L. Qiao, L. Yang, J. J. Zhang, *Adv. Energy Mater.* **2014**, *4*, 1301523.
[7] Y. Y. Liang, Y. G. Li, H. L. Wang, J. G. Zhou, J. Wang, T. Regier, H. J. Dai, *Nat. Mater.* **2011**, *10*, 780 – 786.
[8] Y. Li, Y. Gao, C. Yang, Z. Wang, G. Xue, *Chin. J. Polym. Sci.* **2014**, *32*, 711 – 717.
[9] A. Awadallah-F, T. B. Mostafa, *Chin. J. Polym. Sci.* **2015**, *33*, 376 – 385.
[10] W. Yuan, Y. Zhou, Y. Li, C. Li, H. Peng, J. Zhang, Z. Liu, L. Dai, G. Shi, *Sci. Rep.* **2013**, *3*, 2248.
[11] Y. Li, W. Zhou, H. Wang, L. Xie, Y. Liang, F. Wei, J. Idrobo, S. J. Pennycook, H. Dai, *Nat. Nanotechnol.* **2012**, *7*, 394 – 400.
[12] M. Kaukonen, R. Kujala, E. Kauppinen, *J. Phys. Chem. C* **2012**, *116*, 632 – 636.
[13] H. Kim, K. Lee, S. I. Woo, Y. Jung, *Phys. Chem. Chem. Phys.* **2011**, *13*, 17505 – 17510.
[14] D. Qu, *Carbon* **2007**, *45*, 1296 – 1301.
[15] J. Wu, L. Ma, R. M. Yadav, Y. Yang, X. Zhang, R. Vajtai, J. Lou, P. M. Ajayan, *ACS Appl. Mater. Interfaces* **2015**, *7*, 14763 – 14769.
[16] M. H. Seo, S. M. Choi, E. J. Lim, I. H. Kwon, J. K. Seo, S. H. Noh, W. B. Kim, B. Han, *ChemSusChem* **2014**, *7*, 2609 – 2620.
[17] E. J. Biddinger, U. S. Ozkan, *J. Phys. Chem. C* **2010**, *114*, 15306 – 15314.
[18] L. F. Lai, J. R. Potts, D. Zhan, L. Wang, C. K. Poh, C. H. Tang, H. Gong, Z. X. Shen, J. Y. Lin, R. S. Ruoff, *Energy Environ. Sci.* **2012**, *5*, 7936 – 7942.
[19] A. L. Higginbotham, D. V. Kosynkin, A. Sinitskii, Z. Sun, J. M. Tour, *ACS Nano* **2010**, *4*, 2059 – 2069.
[20] F. J. Martín-Martínez, S. Fias, G. Van Lier, F. De Proft, P. Geerlings, *Chem. Eur. J.* **2012**, *18*, 6183 – 6194.
[21] M. K. Liu, Y. F. Song, S. X. He, W. W. Tjiu, J. S. Pan, Y. Y. Xia, T. X. Liu, *ACS Appl. Mater. Interfaces* **2014**, *6*, 4214 – 4222.
[22] A. Zehtab Yazdi, H. Fei, R. Ye, G. Wang, J. Tour, U. Sundararaj, *ACS Appl. Mater. Interfaces* **2015**, *7*, 7786 – 7794.
[23] Y. Gong, H. Fei, X. Zou, W. Zhou, S. Yang, G. Ye, Z. Liu, Z. Peng, J. Lou, R. Vajtai, B. I. Yakobson, J. M. Tour, P. M. Ajayan, *Chem. Mater.* **2015**, *27*, 1181 – 1186.
[24] K. Sakaushi, T. Fellinger, M. Antonietti, *ChemSusChem* **2015**, *8*, 1156 – 1160.
[25] Z. H. Sheng, L. Shao, J. J. Chen, W. J. Bao, F. B. Wang, X. H. Xia, *ACS Nano* **2011**, *5*, 4350 – 4358.
[26] H. T. Chung, J. H. Won, P. Zelenay, *Nat. Commun.* **2013**, *4*, 1922.
[27] K. Kumar, C. Canaff, J. Rousseau, S. Arriiclacens, T. W. Napporn, A. Habrioux, K. B. Kokoh, *J. Phys. Chem. C* **2016**, *120*, 7949 – 7958.
[28] R. Nie, J. Shi, W. Du, W. Ning, Z. Hou, F. Xiao, *J. Mater. Chem. A* **2013**, *1*, 9037 – 9045.
[29] Q. G. He, Q. Li, S. Khene, X. M. Ren, F. E. López-Suárez, D. Lozano-Castelló, A. Bueno-López, G. Wu, *J. Phys. Chem. C* **2013**, *117*, 8697 – 8707.
[30] J. Wang, J. G. Zhou, Y. F. Hu, T. Regier, *Energy Environ. Sci.* **2013**, *6*, 926 – 934.
[31] L. Lv, T. Ye, L. Gong, K. Wang, J. Su, X. Li, J. Chen, *Chem. Mater.* **2015**, *27*, 544 – 549.
[32] J. Yan, H. Lu, Y. Huang, J. Fu, S. Mo, C. Wei, Y. Miao, T. Liu, *J. Mater. Chem. A* **2015**, *3*, 23299 – 23306.
[33] H. Yu, Y. Li, X. Li, L. Fan, S. Yang, *Chem. Eur. J.* **2014**, *20*, 3457 – 3462.
[34] L. Chen, R. Du, J. Zhu, Y. Mao, C. Xue, N. Zhang, Y. Hou, J. Zhang, T. Yi, *Small* **2015**, *11*, 1423 – 1429.
[35] J. J. Xiao, X. J. Bian, L. Liao, S. Zhang, C. Ji, B. H. Liu, *ACS Appl. Mater. Interfaces* **2014**, *6*, 17654 – 17660.
[36] C. Zhang, M. Antonietti, T. Fellinger, *Adv. Funct. Mater.* **2014**, *24*, 7655 – 7665.
[37] L. T. Qu, Y. Liu, J. B. Baek, L. M. Dai, *ACS Nano* **2010**, *4*, 1321 – 1326.
[38] Y. Y. Jiang, Y. Z. Lu, X. D. Wang, Y. Bao, W. Chen, L. Niu, *Nanoscale* **2014**, *6*, 15066 – 15072.
[39] X. Lu, H. M. Chan, C. Sun, C. Tseng, C. Zhao, *J. Mater. Chem. A* **2015**, *3*, 13371 – 13376.
[40] T. Sharifi, G. Z. Hu, X. E. Jia, T. Wågberg, *ACS Nano* **2012**, *6*, 8904 – 8912.

Manuscript received: June 2, 2016
Revised: August 11, 2016
Final Article published: ■■ ■■, 0000

FULL PAPER

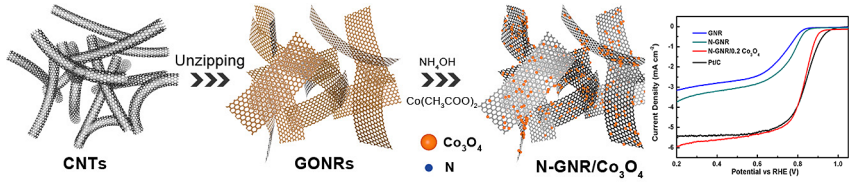

Fuel cell catalysts: A facile, nontoxic one-step hydrothermal method is developed to prepare N-GNR/Co_3O_4 (GNR = graphene nanoribbon) hybrids, which exhibit a comparable oxygen reduction reaction (ORR) onset potential and larger current density compared to commercial Pt/C catalysts with long term stability and excellent tolerance to methanol crossover effects. This work presents a low-cost and sustainable route to prepare efficient noble-metal-free ORR electrocatalysts.

Electrocatalysts

Hengyi Lu, Jiajie Yan, Youfang Zhang, Yunpeng Huang, Wei Gao, Wei Fan, Tianxi Liu**

■■ – ■■

In Situ Growth of Co_3O_4 Nanoparticles on Interconnected Nitrogen-Doped Graphene Nanoribbons as Efficient Oxygen Reduction Reaction Catalyst